CH and C_2 Radicals Characterization in Natural Gas Turbulent Diffusion Flames

C. A. Martins
and A. P. Pimenta
Departamento de Propulsão
Instituto Tecnológico de Aeronáutica
CentroTécnico Aeroespacial
Pça. Mal. Eduardo Gomes, 50, Vila das Acácias
12228-900 São José dos Campos, SP. Brazil
cristiane_andraus@lcp.inpe.br
amilcar@aer.ita.cta.br

J. A. Carvalho Jr.
Universidade Estadual Paulista
Campus de Guaratinguetá
Depto. de Energia
Av. Dr. Ariberto Pereira da Cunha, 333
12500-000 Guaratinguetá, SP. Brazil
joao@feg.unesp.br

M. A. Ferreira
Laboratório Associado de Combustão e Propulsão
Instituto Nacional de Pesquisas Espaciais
Rodovia Presidente Dutra Km 40
12630-000 Cachoeira Paulista, SP. Brazil
marco@lcp.inpe.br

A. A. Caldeira-Pires
Departamento de Engenharia Mecânica
Universidade de Brasília
Campus Universitário Darcy Ribeiro
70910-900 Brasília, DF. Brazil
armandcp@nb.br

This paper reports the construction of an axisymmetric nonpremixed piloted jet burner, with well-defined initial and boundary conditions, known as the Delft burner, to assess turbulence-chemistry interaction in non-premixed turbulent flames. Detailed experimental information is described, involving hot-wire anemometry, thin-wire thermocouples and chemiluminescence visualization measurements. Radial profile of the axial mean velocity indicates excellent agreement between flow patterns developed within Delft installation and the one described herein. Chemiluminescence emissions from CH and C_2 free-radicals were acquired with a CCD camera. Tomography reconstruction analysis was utilised to compare radical emissions and temperature spatial distributions. There was a strong dependence between temperature and CH/C_2 emissions. This is an indication that these radicals can be used in flame front studies.
***Keywords**: Gaseous fuel diffusion flames, flame turbulence, flame tomography, thin-wire termocouples*

Introduction

The present work is motivated by the need to obtain more information about turbulent reacting flows. The initial strategy was to build an installation in which it would be possible to compare results with those obtained by other research groups. The next step was to obtain new data. Our burner is of the same type of that used by the combustion groups at Delft University (Netherlands), Sandia Laboratories (USA), and Sydney University (Australia). In particular, the Delft burner has been designed to produce a number of well-defined turbulent flames of natural gas. The procedure started by comparing the results obtained in our installation and the others. The idea was to identify similarities between them.

In our national context this work has its importance in the increasing use of natural gas as fuel. The government guidelines prescribed increase of the energy share for the natural gas from the current 3 % to 12 % by 2010. Natural gas finds application in different sectors, such as in industrial processes, in vehicles, as household gas and in thermoelectricity plants. In particular, for thermoelectricity the Brazilian Ministry of Mines and Energy created the 2000-2003 Thermoelectricity Priority Program to increase the electric power supply in Brazil. According to the project, 56 thermoelectricity plants will be built by 2003, with a production capacity of around 20.000 MW (Petrobras, 2002).

In this paper, we present first the experimental configurations. Then we discuss measurements of velocities and mean temperatures, which were performed with anemometers and thermocouples, respectively. Tomography analysis was performed to determine the dependence of CH and C_2 radicals luminous intensity with flame height.

Experimental Set-Up

Piloted Jet Diffusion Flame

The measurements were performed in an axisymmetric non-premixed gaseous fuel jet burner. The burner, shown in Figure 1, consists of a round fuel jet outlet with an inner diameter of 8mm and length of 1000 mm. This length is sufficient to establish a fully developed turbulent flow in the nozzle. The burner is operated with primary and secondary air. For the primary air supply, there is an annulus. Its inner and outer diameters are 35 and 45mm,

Paper accepted April, 2005. Technical Editor: Atila P. Silva Freire.

respectively. This burner is mounted in such a way to allow vertical alignment.

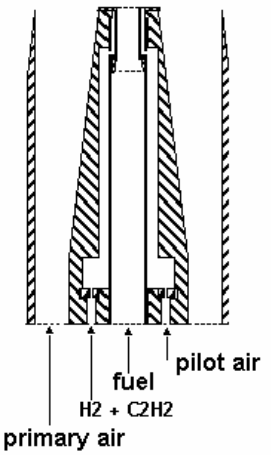

(a)

(b)

(c)

Figure 1. Detail of burner nozzle (a). Twelve holes around the nozzle provide pilot flames (b and c).

Near the nozzle, the inner diameter of the annulus becomes conical with an angle of 7°, leading to an inner annulus diameter of 15 mm at the burner rim. The pilot flame insert is placed at the fuel exit section. The pilot gas issues from twelve 0.5mm diameter holes arranged on a ring, as shown in Figure 1 (b and c). An acetylene/hydrogen/air mixture is used in the pilot flame. The mixture has a C/H ratio equal to that of natural gas, to assure the same basic product composition of the main fuel (as suggested by Starner and Bilger, 1985). The Reynolds number of the pilot flames is about 500 and they are laminar. Their total heat release is about 1% of that of the main flame.

The burner is positioned in an unconfined 0.4 m/s air flow, produced by a wind tunnel with a square exit section with sides of 0.54 m. Figure 2 presents the burner placed in the secondary air flow. This co-flow avoids an external recirculation zone of the combustion products. The throat provides a low velocity ($U \cong 0.4$ m/s) and a low turbulence intensity secondary air flow. The Reynolds number of this secondary co-flow is 15000. Different of the chamber used by De Vries (1994) and Stroomer (1995), our chamber is not octagonal but square. This shape allowed us to have better optical access to the flame. In order to obtain adequate flow characteristics it was necessary to build a settling section. This section contains two screens and two honeycombs. Special care was taken to determine the correct position of the honeycombs because, besides damping the flow, as desired, they may also create unwanted turbulence. We have followed suggestions of Loehrke and Nagib (1976) and Scheiman and Brooks (1981) to define the position of the honeycombs.

The axisymmetry assumption for the experimental apparatus is justified in the following. In fact, there is the possibility of the 12 holes used for the pilot flame to introduce a periodic boundary condition along the inlet plane. Roughly, there are three disturbances that the pilot flame could introduce into the main flame flow. The first is the thermal disturbance, which is directly linked with release of energy from the pilot flame. From a quantitative point of view, there is little influence when the pilot flame has an energy output on the order of only 1% of the main flame. The second is the chemical disturbance, which is minimised with the identical C/H ratio in pilot premixed flame. This results in combustion products of the same basic composition as those of the main fuel. For third and last effect comes from aerodynamics perturbations. The Reynolds number of the pilot flame is on the order 500 at the nozzle exit. Considering the lower natural gas mass flow rate, 0.21 g/s, the exit velocity will be 11 m/s and the Reynolds number, based on the pipe inner diameter, will be 3,900. The aerodynamic effects are more significant when the pilot and the main flame possess similar Reynolds numbers.

An extensive set of data were obtained in early works in which the flame is described as axisymmetric, including laser-Doppler anemometry (LDA) of the flow field (Stroomer et. al, 1999), 2D laser-induced fluorescence (LIF) data on the OH radical concentration (De Vries, 1994), and coherent anti-Stokes Raman spectroscopy (CARS) measurements of the mean temperature and temperature statistics (Mantzaras and Van Der Meer 1997).

Temperature Measurements

Thermocouples are widely used instruments in experimental combustion research. They are used to determine mean and fluctuating values of local temperatures (Turns et al., 1993; Darabiha et al., 1996). In this work, an uncoated platinum-rhodium (13 %) thermocouple wire, with a diameter of 38 μm, was used. The advantage of this alloy is that it can support temperatures up to about 2000 K and also the temperature of the cold junction is not critical for the measurement.

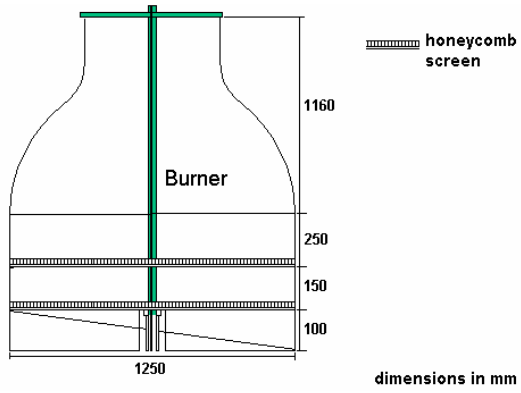

Figure 2. Burner setup with burner placed in a throat for secondary air.

The thermocouple, then, consisted of two 38-μm diameter wires with a length of about 5mm, which were welded together. Heavier thermocouple wires (500μm) were fed through the ceramic probe and acted as support wires for the finer thermocouple wire (38μm) used to form the junction, as shown in Figure 3a. The thermocouple ceramic tube was placed in a steel holder, which was mounted in the traversing unit. The accuracy of the thermocouples position co-ordinates was 1mm in axial direction, relative to the burner, and 0.1 mm in the radial direction. The wires were welded together, forming a junction only slightly larger than the thermocouple wires. The equipment used is an adaptation of an anemometry welding system. Figure 3b shows a welded junction.

The data were recorded with a National Instruments SCII 100 32 channel input board. The rejection rate used was 100 dB at 100 Hz and 20 dB at 1 MHz. The sample frequency was about 5 kHz at every position; the measured value was an average of 1000 measurements.

The main advantages of thermocouples are their ease of use, low cost and good time and space resolution. The limitations are the thermocouple errors linked to probe aerodynamics and thermal and chemical effects. In general, these limitations lead to systematic errors.

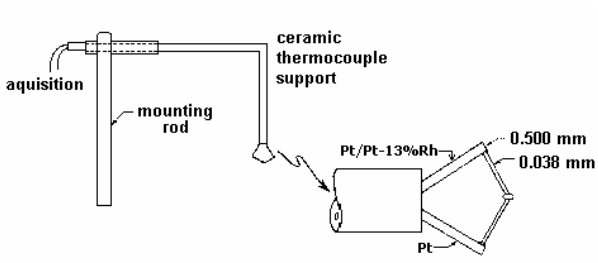

(a)

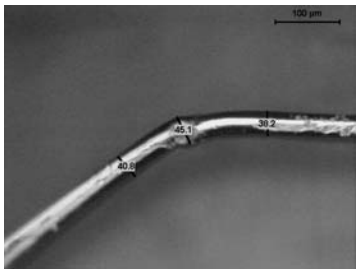

(b)

Figure 3. Probe thermocouple setup (a); thermocouple junction, approximately 200 times, by Leica Microscopic (b).

A probe inside a flow causes local and global field disturbances of either aerodynamic, thermal or chemical nature. The aerodynamic disturbances are considered to be the most serious. They may be minimised by adequate probe design, which includes decreasing the size of the probe and considering problems of fabrication and wire fragility. The thermal effects consist of the probe acting as a heat sink; they are function of the temperature difference between the stream and the sensor. The chemical effects are basically caused by catalytic effects which increase the reaction rates of the flame chemistry. This last effect can be negligible by coating the thermocouple with non-catalytic silica, but this introduces additional uncertainties and it is therefore not used.

The thermal disturbances are result of heat transfer between the thermocouple and its surroundings. Conduction losses are negligible if the wire length is larger than 160 times its diameter (Moneib, 1980). Our thermocouple probe is 10 mm long and its diameter is 0.038 mm.

Usual radiation corrections take the form of (Bradley and Matthews, 1968):

$$T_g = T_t + \frac{\sigma \varepsilon_t T_t^4}{h_t}, \qquad (1)$$

where T_g is the actual gas temperature, T_t is the measured thermocouple temperature, ε_t is the emissivity of the thermocouple junction, σ is the Stefan-Boltzman constant ($5.67\ 10^{-8}$ W/m^{2}K^4), and h_t is the heat transfer coefficient at the wire surface.

For the Pt/PtRh13% alloy the emissivity is not reported, and therefore the emissivity of the thermocouple is calculed based to be in emissivity of a Pt/PtRh10%. Bradley and Entwistle (1961) showed that the emissivity increases with the ratio rhodium to platinum. Hence, the emissivity of our thermocouple is expected to be larger for Pt/PtRh10%. An expression for the wire emissivity working with thermocouples and temperatures above 1250 K is:

$$\varepsilon_t = 9.35 10^{-5} T_t + 0.06 \qquad (2)$$

Actual values of ε_t are in the range 0.20-0.40.

The convective heat transfer coefficient at the wire surface h_t can only be estimated from the Nusselt relation from Bradley and Matthews (1968):

$$Nu = \frac{h_t D_t}{\lambda_g} = 0.42\,\mathrm{Pr}^{0.2} + 0.57\,\mathrm{Pr}^{0.33}\,\mathrm{Re}^{0.5}, \qquad (3)$$

valid for $0.01 < \mathrm{Re} < 10^4$, where Re and Pr are Reynolds and Prandtl dimensionless numbers. The parameter λ_g is the thermal conductivity coefficient and it can be estimated from flue gas properties:

$$\lambda_g = 3.75 10^{-5} T_t + 0.04 \quad [\mathrm{W/mK}] \qquad (4)$$

where T_t is the temperature measured by the thermocouple.

Once the Pr and Re are known, an equation for h_t can be derived. The Prandtl number is given by

$$\mathrm{Pr} = \frac{\nu}{a}, \qquad (5)$$

where ν is the kinematic viscosity a is the thermal diffusivity, estimated by:

$$\nu = 2.5x10^{7} T_t - 1.43x10^{-4} \quad [\mathrm{m^2/s}] \qquad (6)$$

and

$$a = 2.89x10^{-7} T_t - 1.22x10^{-4} \qquad (7)$$

The Reynolds number is

$$\mathrm{Re} = \frac{\bar{u} D_t}{\nu} \qquad (8)$$

where $\bar{u}$ is the mean velocity and D_t is the diameter of the thermocouple wire. The equation for the convective heat transfer coefficient h_t becomes, then:

$$h_t = \frac{\lambda}{D_t} 0.42 \left(\frac{\nu}{a}\right)^{0.20} + 0.57 \left(\frac{\nu}{a}\right)^{0.33} \left(\frac{\bar{u} D_t}{\nu}\right)^{0.50} . \qquad (9)$$

With this equation, Equation (1) can be solved and the effects of radiation and convection are accounted for. Corrections for the obtained mean temperatures in flame measurements range from 15 K for temperatures of 500 K, to 100 K for temperatures of 1750 K. From the scattering of the data, the remaining experimental accuracy is estimated to be ± 70 K.

Flow Configurations

The fuel was bottled natural gas from Bolivia (GASBOL). The fuel installation contains 6 bottles which withstand pressures up to 180 bar. The GASBOL is composed of mainly methane (88.27%) and ethane (7.67%). The net lower calorific value is 49.1 MJ/kg. The density is $\rho = 0.74 kg/m^3$. Air is supplied from a compressed air line. The density of air is 1.20 kg/m^3 (1 atm and 293K). The accuracy of the fuel and primary air flow rates are about 2 % and 5 % respectively. Table 1 shows the conditions for two analysed flames:

Table 1. Conditions for two analysed flames. Subscripts j and a denote the fuel nozzle and the primary air annulus exit, respectively.

Flame	Fuel				Primary air			
	(g/h)	Uj (m/s)	Tj (K)	Rej (10^3)	(g/h)	Uj (m/s)	Tj (K)	Rej (10^3)
1	750	10.85	298	3.9	14360	2.17		0,9
2	1050	15.34	298	5.4	18102	3.14		1.0

Velocity Measurements

In this work the velocity measurements were conducted with a hot-wire anemometry (HWA) probe. Anemometry is an indirect measuring technique, i.e., requires calibration in a known flow field before it can be applied to fluid flow velocity measurements. The wire of a typical HWA has a diameter of 5 μm and temperature of 150 to 300 °C during operation. The correlation between the flow velocity and heat transfer rate has been approached mainly empirically and the form of the calibration equations was derived from a large number of experiments (Lange et al. 1999). The experimental set-up used to obtain the velocity field is presented in Figure 4.

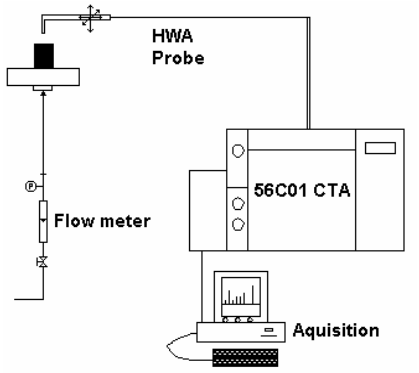

Figure 4. Schematic representation of the HWA configuration.

Measurements in isothermal jets have been obtained under the conditions presented in Table 2. For jets I and II, the air flow rates for the jet section, $\phi_{air,jet}$, and the annulus section, $\phi_{air,ann}$, are given with the respective exit velocities and Reynolds numbers. Jet I is an air into stagnant air.

Table 2. Flow settings for the isothermal jets.

Jet	$\phi_{air,jet}$ (g/s)	$U_{air,\ jet}$ (m/s)	$Re_{air,\ jet}$	$\phi_{air,ann}$ (g/s)	$Re_{air,\ ann}$ (m/s)
I	0.74	21.8	8.7×10^3	0.0	0
II	0.74	21.9	8.7×10^3	4.3	8.6×10^3

Both jets I and II data can be compared with Delft data. This comparison is shown in Figures 5 and 6. For the Delft experiments the velocity measurement was performed with the Laser Doppler Anemometry technique (Stroomer, 1995). The statistical uncertainties, with a 95 % confidence interval, were ± 1 % and ± 1.5 % for the mean axial and radial velocities, respectively. For our hot wire anemometer, for a 95 % confidence interval including the calibrator uncertainty, the uncertainty was 3%. Several options are available for plotting/comparing the methods, depending on the best estimation of the true values. Appendix A shows some plots that allow visual assessment of the agreement (or disagreement) between both. The choice is to plots the difference between methods against the mean values achieved by the methods. The mean values of the methods are regarded as the best estimation of the true values. The two methods can be compared for bias and agreement. Just one example is shown, but all results allowed the same conclusions. Similarity and good agreement can be observed between both flow configurations.

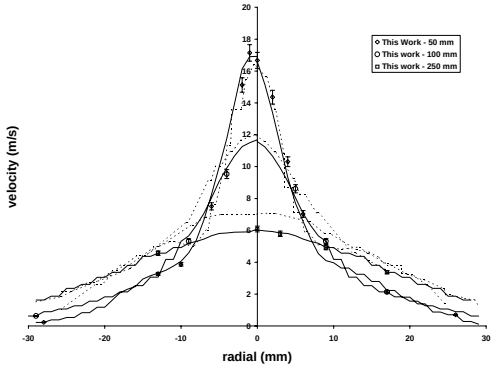

Figure 5. Radial mean velocity profiles in jet I at axial distance from the nozzle y = 50, 100, and 250 mm. ____ This work and ----- Delft Installation (Strommer, 1995).

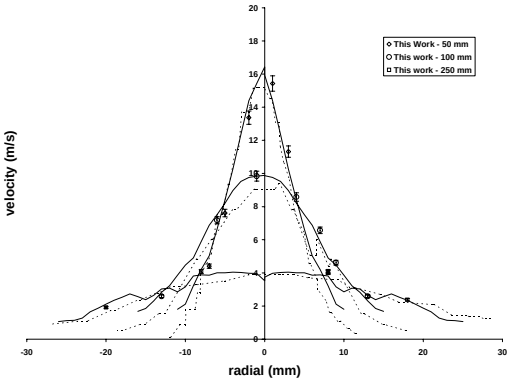

Figure 6. Radial mean velocity profiles in jet II at axial distance from the nozzle y = 50, 100, and 250 mm. ____ This work and ----- Delft Installation (Strommer, 1995).

Kinetics Studies with the Chemkin Code of CH, C_2 and OH Radicals

Probably the most familiar free-radical reaction for most people is combustion. In order for combustion to occur the relatively strong O=O double bond must be broken to form oxygen free radicals. The flammability of a given material is strongly dependent on the concentration of free radicals that must be obtained before initiation and propagation reactions dominate leading to combustion of the material. Once the combustible material has been consumed, termination reactions again dominate and the flame dies out.

In chemistry free radicals are atomic or molecular species with unpaired electrons or an otherwise open shell configuration. Unpaired electrons make the species more attracted to a magnetic field (they are said to be paramagnetic). This gives free radicals a highly reactive nature. They are capable of independent existence and act as intermediates in chemical reactions. Although they have the ability to exist independently they usually have a fleeting existence. Free radicals play an important role in combustion, atmospheric chemistry and many other chemical processes.

Reactions involving free radicals are usually divided into three categories: initiation, propagation, and termination. The initiation step is responsible for the initial decomposition of the reactants. Propagation steps involve a radical-molecule reaction with generation of a radical in the product, while branching reactions produce two radicals per single radical in the reactants. The generation of a flame is due to branching reactions predominating over termination, with a large generation of radicals resulting in the fast decomposition of the fuel.

The CHEMKIN 3.6 package (Kee et al., 2000) was used to investigate the kinetic behaviour of the CH, C_2 and OH radicals. The detailed mechanism was based on the GRI-Mech 3.0 (1997) for natural gas. The model used was a planar diffusion flames between two opposing nozzles, air and fuel, in accordance with Puri et al. (1987) and Lutz et al. (1997). The burner for which the CHEMKIN was used is completely different of the burner of the present experimental investigation. The idea was to find a correlation for the temperature and the radicals. Figure 7 shows the diagram of the flow investigated with the computer package.

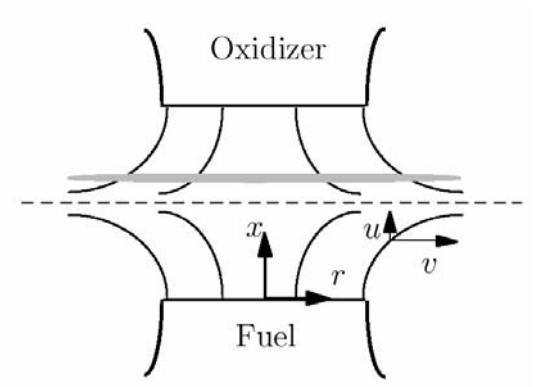

Figure 7. Schematic diagram of opposed-flow diffusion flame (adapted from Lutz et al., 1997).

Figure 8 presents the variation of C_2, CH and OH concentrations and gas temperature along the axis that links the oxidiser and fuel outlets. This figure indicates that the correlation between the C_2/CH radicals and the temperature is stronger than that for the OH radical and the temperature. This fact suggests that the two first radicals represent a more precise signature of the reaction zone.

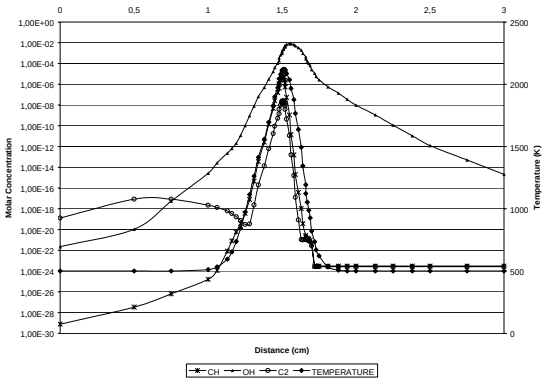

Figure 8. Variation of the CH, C2 and OH radical concentrations and the temperature with the axial distance for a opposed-flow flame.

One observation it is about the scale of the Figure 8. It is clear that 1E-30 is completlly out of the physical meaning. But the idea is only shows the qualitative similarity between radicals behaviour and temperature and the visualisation became better when the scale is used for.

Image Acquisition

The image acquisition system comprises a CCD Marshall Camera (8 bits, 520 x 480 pixels) and a Fujinon CF 50 B lens (f 1:1.4/50). Images were acquired as mean images, calculated according to the following equation:

$$\bar{I}_{pixel} = \frac{\sum_{i=0}^{N} I_i}{N}, \qquad (10)$$

where $\bar{I}_{pixel}$ stands for the mean intensity of the *n* pixel, N for the number of images, and I_i for the pixel intensity. Moreover, the images ensemble turbulence intensity (showed in terms of the root mean square value) is calculated as

$$RMS = \frac{\sqrt{\frac{\sum_{i=1}^{N}(I_i - \bar{I})^2}{N}}}{\bar{I}}. \qquad (11)$$

Figure 9 shows the evolution of the mean and rms values of light intensity, as acquired by a specific pixel of the CCD array. It can be depicted that after 100 images the rms of the average image does not vary significantly.

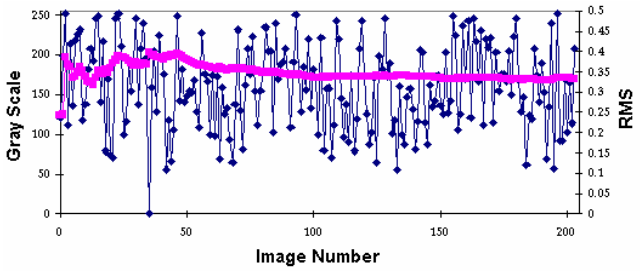

Figure 9. Evolution of the time-resolved intensity and rms values with number of images in the pixel 144,100.

Figure 10 shows a scheme of the experimental apparatus to obtain the image at different positions in the flame. In this way, four cameras were aligned. Image acquisition was obtained with lower perturbation. Tests were designed to quantify the response of each one of the camera assemblies. The consistence of the yielded results was verified by comparison of the results obtained with all the assemblies. Additionally, diaphragm corrections were necessary and they were performed. Details of procediments are described in Andraus (2003).

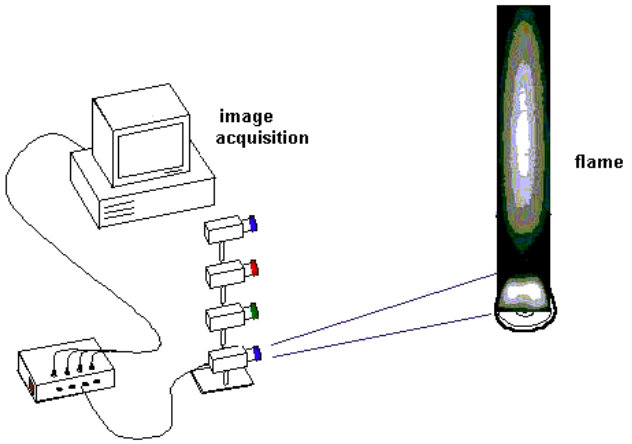

Figure 10. Scheme for image acquisition at different flame positions.

Figure 11 presents different regions where the image were acquired for each camera. Each camera it able to view 15 cm in the flame length.

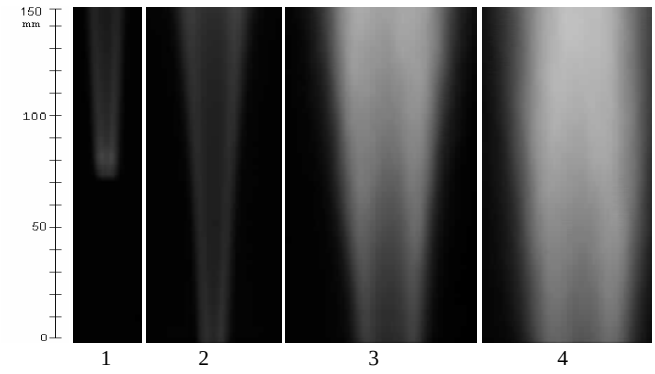

Figure 11. Images obtained by cameras 1, 2, 3, and 4, respectively. Camera 1 is at the bottom.

The images were acquired in two wavelengths: 432.22 and 514.99 nm. The first is characteristics of the CH radical and other of the C_2 radical.

Tomographic Reconstruction Algorithms

Tomographic reconstruction of local flame emission is based on the deconvolution of a finite number of two-dimensional path integrated measurements of radiative flame intensity, as described by Caldeira-Pires (2001). In this work, tomographic reconstruction is based on monochromatic radiation data acquired making use of the aforementioned CCD cameras and the specific pass-band filters centred on CH and C2 main chemiluminescence band.

In this context, the purpose of tomographic reconstruction is to obtain the original distribution, *F(x,y)*, from the various projections, *P(p,ϕ)*, and in particular, for an axissymmetric object, to obtain *F(r)* from *P(p)*. This can be accomplished by making use of the Inverse Abel Integral Equation.

In order to minimize the errors associated to the inversion of Abel's transform along the axis of symmetry, Gordon et al. (1970) described a method similar to an Algebraic Reconstruction Technique (ART), where this limitation has been overcome by using a numerical interpretation of the reconstruction procedure. In this sense, an axissymmetric flame can be modeled as a set of layers, within which all scalar properties are constant. While crossing the flame, the emitted radiation is assumed to have no attenuation by absorption.

For axissymmetric unconfined systems, the integrated intensity values detected by each element of the image collection system, P_j, are a function of the local intensities in the flame, F_i, and the intersection areas, quantified by the coefficients, A_{ij}, such that

$$f_i^{(r+1)} = f_i^{(r)} + \lambda . a_{ij} \frac{p_j - \sum_i a_{ij} f_i^{(r)}}{\sum_j a_{ij}^2} . \qquad (12)$$

In this equation, the difference $p_j - \sum a_{ij} f_i^{(r)}$ represents the error between the correct projection value, P_j, and the re-projection of the image estimate, F_i, after '*r*' iterations. $\sum_j a_{ij}^2$ is a normalization factor, and the correction (the term between square brackets) is backdistributed to the image samples, F_i, along the ray according to the weighing coefficients, A_{ij}. Relaxation factor (λ) can be varied between steps and may be chosen in the range 0.0 to 2.0, in order to improve convergence.

Improved reconstructed images can be obtained by combining correction terms from all rays within a particular projection before the image function is updated. The approach, initially derived by Andersen and Kak (1984), is referred to as the simultaneous algebraic reconstruction technique, SART, and leads to an update-correction strategy defined as:

$$f_i^{(r+1)} = f_i^{(r)} + \lambda \frac{\sum_j a_{ij} \Delta_j}{\sum_j a_{ij}} , \qquad (13)$$

and

$$\sum_j a_{ij} \Delta_{ij} = \sum_j \left[a_{ij} \frac{p_j - \sum_i a_{ij} f_i^{(r)}}{\sum_i a_{ij}} \right] . \qquad (14)$$

This approach has been implemented by Caldeira-Pires et al (2003), and used to reconstruct CH and C2 projections acquired throughout this study. Figure 12 shows a projection, the reconstructed image and the intensity amplitude profile of a specific CCD line for the C2 radical.

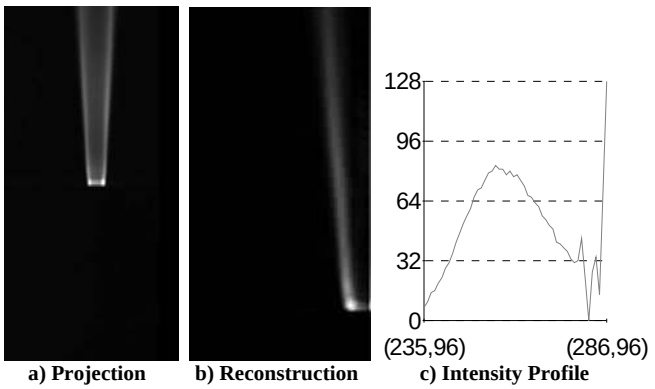

Figure 12. Chemiluminescence analysis of a natural gas flame; C_2 radical. a) projection using camera at position 1; b) tomographic reconstruction; c) intensity amplitude profile at CCD line 96, arbitrary units.

Results

The main objective of this work was to identify qualitative similarities between mean temperatures and CH and C_2 intensities. First, these radicals are abundant in hydrocarbon combustion and, second, average temperature measurements are relatively easy to obtain. There is an observation related to the use of the equipment, the CCD cameras, which do not furnish fluctuation values due to instrument limitations. Fluctuations measurements are possible only with different and more expensive one another experiments when there are necessity of the different and more expensive instruments.

Fluctuating temperature results would allow interesting comparisons. However, the particular idea of this work is to raise the possibility of conducting direct measurements of radical intensity to obtain direct relations with temperature and, in consequence, obtain a better definition of the reaction zone.

In the analysed flow condition the major velocity gradient occurs in the region between central fuel jet and the primary annular air flow. Once mixing between the reactants is sufficiently established, the combustion reaction and the heat release occur, resulting in high temperatures in a narrow region.

Combustion influences turbulence through increased viscosity and decreased density in the regions of the flame with high temperature. Decrease of the level of turbulence in the flame is due to the increased viscosity, especially near the region where the temperatures are highest. This effect is discussed by Takagi et al. (1980) and Sislian et al. (1988). The reaction zone in a natural gas flame is at a (low) mixture fraction of 0.07, implying that, in the radial direction the reaction zone is close to the outer boundary of the fuel jet shear layer. In this section we discuss the average temperature results, measured with thin thermocouples, and related them to the CH and C_2 emissions.

Since the obtained results were similar for the two flow configurations, we selected flame I for the discussion. The analysed flame presented a high maximum average temperature (1900 K) already at the axial coordinate of 50 mm. This is due to the relative low Reynolds number (about 4000) and also the hot products from the pilot flames, which can be transported more slowly in the lower Reynolds number flame. This may also contribute to the high temperature close to the nozzle.

The maximum CH and C_2 intensity are correlated with the maximum average temperature at the corresponding axial locations. C_2 and CH radicals are found in the regions with highest temperatures at different axial locations. High temperature and CH and C_2 are expected in the narrow reaction zone and certain correspondences among the maximum average temperature and maximum CH and C_2 emission intensities are expected. Considering the Chemkin simulation, showed in Fig.8, a higher degree of similarity could be expected between the CH/C_2 and the temperature profiles than between the OH and temperature profiles.

Figures 13 and 14 compare the profile of CH and C_2 with profile temperature in flame I at y = 50 mm, 100 mm and 150 mm. Figure 13 shows that both the maximum C_2 emission and the maximum average temperature decrease with the axial distance. Also, it can be observed, in the rich side, the maxima C_2 and temperature for the same radial location, 50 mm. The CH profile presents a different behaviour. For increasing axial distance, there is an increase of concentration until 100 mm. Then the emission then decreases. After 200 mm the profile is similar to that observed for the range 200-300 mm, as shown in Figs. 15 and 16.

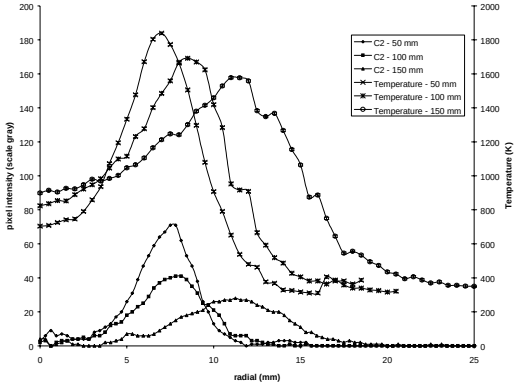

Figure 13. C2 emission and temperature profiles for flame I at 50, 100, and 150 mm longitudinal locations.

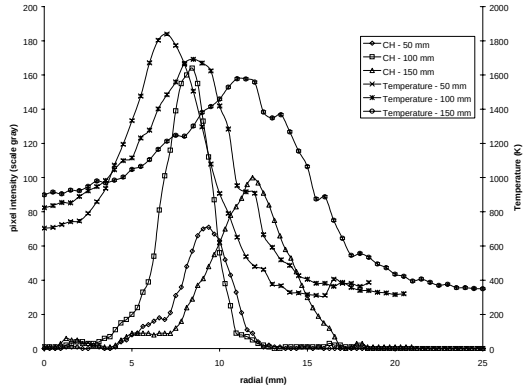

Figure 14. CH emission and temperature profiles for flame I at 50, 100, and 150 mm longitudinal locations.

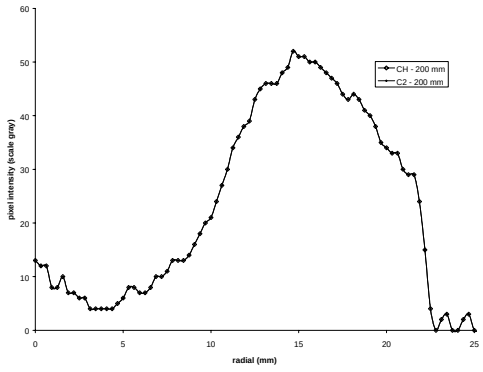

Figure 15. CH and C_2 emission profiles in flame I at 200 mm.

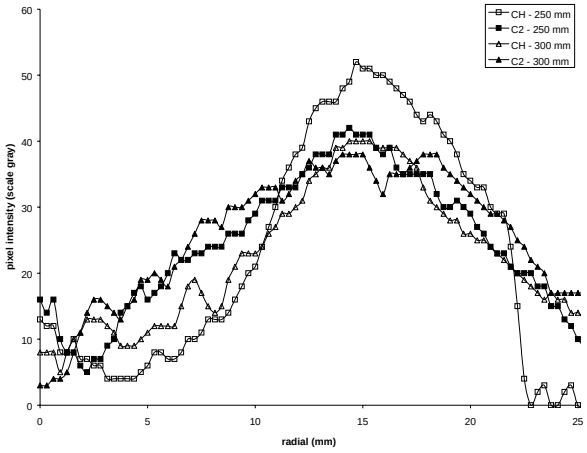

Figure 16. CH and C_2 emission profiles in flame I at 250 mm and 300 mm.

Conclusion

Measurements of the mean temperature and CH profile provide information on the position of the reaction zone and influences on the flame structure. Combustion reactions and heat release occur in a thin interfacial region between the fuel and the primary air stream.

The exact position of the flame front, which is identified by the maximum heat release, is of major interest when investigating the turbulence flame interaction. In turbulent jet flames, an important source of turbulence is caused by turbulence shear layers. The interaction between turbulent eddies an the reaction zone results in displacement and stretching of the reaction zone. Also, the reaction zone can be broadened by diffusion. According to Peters (1991), a characteristic time scale of diffusion, determining the width of the reaction zone of a laminar diffusion flame, is the inverse of the dissipation rate which is proportional to the strain rate or local velocity gradient. The flame analysed here has a relatively small Reynolds number. The local velocity gradients decrease more strongly with the axial position in this flow condition. This flame broadening in zone reaction is clear. Broadening regions of CH and C_2 can be observed as the axial position increases. Chemkin simulation showed that CH and C_2 profiles are closer to the temperature profile than the OH profile. Following, the CH and C_2 profile intensities were correlated with that of the temperature profile. The peak of CH occurred at the position of 100 mm. Then, the CH intensity decreased. At 200 mm, the CH and C_2 emission intensities were practically the same. This indicates that the reaction zone stops between 150 and 200 mm. The spectrum of the CH radical depends strongly on temperature; therefore it can be used for temperature measurements in flames.

Acknowledgement

The authors are grateful to FAPESP (Fundação de Amparo à Pesquisa do Estado de São Paulo) for the support of this work through projects 98/15539-0 and 96/10310-0.

References

Andersen, A.H.; Kak, A.C., Simultaneous algebraic reconstruction technique (SART): a superior implementation of the ART algorithm, *Report*, School of Electrical Engineering, Purdue University, 81-94, 1984.

Andraus, C.A.M., "Investigação da Formação do Poluente NO_x em Chamas Turbulentas Sem Pré-Mistura", Tese de Doutorado, Instituto Tecnológico de Aeronáutica, 2003

Bland, J.M.; Altman D.G., Statistical methods for assessing agreements between two methods of clinical measurement, *The Lancet*, 307-310, 1986.

Bradley, D.; Entwistle, A.G., Determination of the emissivity, for total radiation, of small diameter Platinum-10%Rhodium wires in the temperature range 600-1450 °C, *British Journal of Applied Physics*, 12, 708-711, 1961.

Bradley, D.; Matthews, K.J., Measurement of hight temperatures with fine wire thermocouples, *Journal Mechanical Engineering Science*, 10, 299-305, 1968.

Caldeira-Pires, A.A., Free radical imaging techniques applied to hydrocarbon flame diagnosis, *Journal of Thermal and Fluid Sciences*, 10(2), 132-145, 2001.

Caldeira-Pires, A.A.; Roque, B.R.; Araújo, M.A., 2D Fan Tomographic Reconstruction of Flame Chemiluminescent Emission, *17th Brazilian Congress of Mechanical Engineering*, to be presented, 2003.

Darabiha, N.; Candel, S.; Wirth, D.A.; Mahan, J.R., Numerical studies of a pulsating burner-stabilized laminar premixed methane-air flame, *Combustion Science and Tecnology*, 113-114, 35-47, 1996.

De Vries, J.E.; Study on turbulent fluctuations in diffusion flames using laser induced fluorescence, *Doctorate Thesis*, Delft University of Technology, 1994.

Gordon, R.; Bender, R.; Herman, G., Algebraic reconstruction techniques (ART) for three-dimensional electron microscopy and X-ray photography, *Journal of Theoretical Biology*, 29, 471-481, 1970.

Kee, R.J.; Rupley, F.M.; Miller, J.A.; Coltrin, M.E.; Grcar, J.F.; Meeks, E.; Moffat, H.K.; Lutz, A.E.; Dixon-Lewis, G.; Smooke, M.D.; Warnatz, J.; Evans, G.H.; Larson, R.S.; Mitchell, R.E.; Petzold, L.R.; Reynolds, W.C.; Caracotsios, M.; Stewart, W.E.; Glarborg, P.; Wang, C.; Adigun, O., *CHEMKIN Collection, Release 3.6*, Reaction Design, Inc., San Diego, CA, 2000.

Lange, C.F, Durst, F.; Breuer, M., Wall effects on heat losses from hot wires, *International Journal of Heat and Fluid Flow*, 20, 34-37, 1999.

Loehrke, R.I.; Nagib, H.M., Control of free-stream turbulence by means of honeycombs: a balance between suppression and generation, *Journal of Fluids Engineering*, 1976.

Lutz, A.E.; Kee, R.J.; Grcar, J.F.; Rupley, F.M., Oppdif: a Fortran program for computing opposed-flow diffusion flames, *Sandia Report Sand96-8243*, 1997.

Mantzaras, J.; Van Der Meer, T.H. Coherent anti-stokes Raman spectroscopy measurements of temperature fluctuations in turbulent natural gas-fueled piloted jet diffusion flames. Combustion and Flame, v. 110, n. 1-2, p. 30-53, jul. 1997.

Moneib, H.A., Experimental study of the fluctuating temperature in inert and reacting turbulent jets, *Doctorate Thesis*, Imperial College of Science and Technology, 1980.

Peters N., Length Scales in Laminar and Turbulent Flames, *Progress in Astronautics and Aeronautics*, 135, 155-182, 1991.

Petrobras, 2002: http://www.petrobras.com.br

Puri, I.K.; Seshadri, K.; Smooke, M.D.; Keyes, D.E., A comparison between numerical calculations and experimental measurements of the structure of a counter-flow methane-air diffusion flame, *Combustion Science and Technology*, 56, 1-22, 1987.

Scheiman, J.; Brooks, J.D., Comparison of experimental and theoretical turbulence reduction from screens, honeycomb, and honeycomb-screen combinations, *Journal of Aircraft*, AIAA 80-0433R, 18 (8), 638-643, 1981.

Sislian, J.P.; Jiang, L.Y.; Cusworth, R.A., Laser Doppler velocimetry investigation of the turbulence structure of axisymmetric diffusion flames, *Progress in Energy and Combustion Science*, 14(2), 19-146, 1988.

Starner, S.H.; Bilger, R.W., Characteristics of a piloted diffusion flame designed for study of combustion turbulence interactions, *Combustion and Flame*, 61, 19-38, 1985.

Stroomer, P.P.J., Turbulent and OH structures in flames, *Doctorate Thesis*, Delft University of Technology, 1995.

Stroomer, P. P. J.; De Vries, J. E.; Van Der Meer, T.H. Effects of small - and large-scale structures in a piloted jet diffusion flame. Flow Turbulence and Combustion, v. 62, n. 1, p. 53-68, 1999

Takagi T.; Shin H.D.; Ishio A., Local laminarization in turbulent diffusion flames, *Combustion and Flame*, 37, 163-170, 1980.

Turns, S.R.; Myhr, F.H.; Bandaru, R.V.; Maund, E.R., Oxides of nitrogen emissions from turbulent jet flames: part II – fuel dilution and partial premixing effects, *Combustion and Flame*, 93, 255-269, 1993.

Appendix A

A more detailed analysis of the velocity measurements is provided in this Appendix. The objective is compare data obtained in this work with those obtained by Strommer (1995). Strommer's measurements were performed with the Laser Doppler Anemometry technique, while this work utilised the Hot-Wire Anemometry

(HWA) technique. An example follows, in which the values obtained with both techniques are compared. All the other measurements yielded similar comparison.

The method utilised to perform the comparison is known as Bias plots. Bland and Altman (1986) suggest that the mean of the observations of two methods is considered as the best estimation of the true value. If the methods are comparable, observations should closely follow the identity line. Figure A1 shows very good similarity between both. The identity line is A = B. Figure A2 indicates the existence of an insignificant bias between the methods, since the horizontal line through 0 is contained within the 95% confidence interval limits.

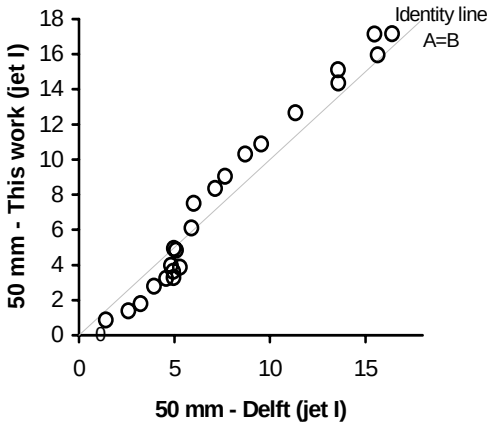

Figure A1. Comparison between two methods (results obtained within 95% confidence interval; lower: -2.266, should be between –3.112 and –1.419; upper: 2.486, should be between 1.639 to 3.332).

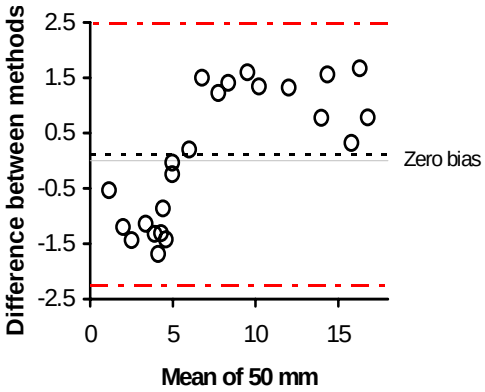

Figure A2. Bias of method B compared with method A (results obtained within 95% confidence interval; dashed line is at 0.110, should be between -0,414 to 0,634.).

The dashed line shows the bias of method B (this work) compared with method A (Delft). The continuous line indicates zero bias. In the example the bias is + 0,110, so the average observations of this work are 0,110 higher than observations made using Delft methods. The dotted/dashed line shows the 95% limits of agreement. If the differences are normally distributed, 95% of the differences will likely lie within the range.